



Contents lists available at ScienceDirect

Calphad

journal homepage: <http://www.elsevier.com/locate/calphad>

# Thermodynamic reassessment of the Ag–Cu phase diagram at nano-scale

M.Z. Chu, Y.Z. Qin, T. Xiao, W. Shen, T. Su, C.H. Hu, Chengying Tang \*

School of Materials Science and Engineering & Guangxi Key Laboratory of Information Materials, Guilin University of Electronic Technology, Guilin, Guangxi, 541004, PR China

## ARTICLE INFO

### Keywords:

Ag–Cu nanoalloys  
Surface effect  
Thermodynamic assessment  
Phase diagram

## ABSTRACT

The Ag–Cu phase diagram at nanoscale was reassessed by CALculation of PHase Diagrams (CALPHAD) method, considering the surface effect on the chemical potential of pure substance and excess Gibbs free energy of mixtures. According to the reported thermodynamic properties of pure Ag and Cu nanoparticles (NPs), and the measured melting eutectic temperatures of  $\text{Ag}_8\text{Cu}_2$ ,  $\text{Ag}_7\text{Cu}_3$ ,  $\text{Ag}_6\text{Cu}_5$  to  $\text{Ag}_5\text{Cu}_5$  NPs, respectively, obtained in the previous works, self-consistent thermodynamic parameters including the size effect were obtained by thermodynamic optimization. Using the obtained thermodynamic parameters, four Ag–Cu nano phase diagrams were constructed, and thermodynamic properties were calculated. It was indicated that the calculated Ag–Cu nano phase diagrams agreed well with experimental data.

## 1. Introduction

Nanomaterials, showing unique size-dependent physical, chemical and thermodynamic properties, have received intensive attention across several disciplines in past decades [1–7]. It has been found that a decrease in particle size leads to the melting temperature depression and therefore, in nanomaterials, the phase transition temperature decreases in comparison to that of the bulk material [8–10], indicating the increase of the Gibbs free energy of surface of a nanosized system due to the size and shape effects [11–15]. Hence, the phase diagram for the bulk cannot satisfy the design and practical application of nano system. The phase diagram at nanoscale and the thermodynamic properties for describing the phases of nano system should be re-evaluated and re-optimized by considering the reported experimental results and size effect on the surface energy. Since the easy aggregation of nanomaterials leads to technical difficulties in the experimental determination of their thermal stability, theoretical models are generally used to predict thermodynamic properties. Several theoretical works by molecular dynamic simulations [16,17] and thermodynamic modeling [18,19] have been reported. In the early twentieth century, Pawlow [20] first proposed the thermodynamic model of the nano system to theoretically predicted the size-dependent melting point depression, which was originally confirmed by Takagi's experimental observations using a transmission electron microscope [21]. Then, different techniques such as electron diffraction [22], X-ray diffraction [23], and calorimetric measurements [24] have been used to clarify the relationship between

the melting points and the particle size. The CALPHAD method has been recognized to be useful in various aspects of materials science and engineering [25]. It was found that the modified method of nano-CALPHAD [26] has been employed to predict theoretically the melting points depression and phase diagram equilibrium [27,28] of nano systems.

Ag–Cu nanoalloys have attracted great attention due to its unique properties if used in optoelectronics [29], catalysis [30], and biomedicine [31]. Because of its promising electrical and thermal conductivity coefficients, Ag–Cu nanoparticles (NPs) have been recommended as an alternative used to connect electronic components as lead-free solder [32,33]. By evaluating the phase equilibria with an emphasis on the adsorption behavior based on Butler's equations, Hajra and Acharya [34] investigated the thermodynamics and phase equilibria of Cu–Ag nano system involving nano phases of 1 nm. Although a considerable decrease in the melting points of the pure components and alloys was reflected, their calculated results disagreed with the experimental data on melting of Ag [35], Cu [36], and Ag–Cu alloys [37], reported later in literature, since no temperature coefficients and molar volumes of pure solid metals were not available. Huang et al. [38] experimentally obtained a 75 K depression of eutectic melting point of Ag–Cu nanoalloys employed the experimental data with the size of 10 nm in the carbon shells. By using the model suggested by Lee [39], Garzel et al. [40] reassessed the phase diagram of Ag–Cu systems including particle size and shape effect. Using the obtained thermodynamic parameters, two phase diagrams with sizes of 10 nm and 100 nm were, calculated,

\* Corresponding author.

E-mail address: [ctang@guet.edu.cn](mailto:ctang@guet.edu.cn) (C. Tang).

<https://doi.org/10.1016/j.calphad.2020.102233>

Received 17 September 2020; Received in revised form 26 November 2020; Accepted 26 November 2020

Available online 9 December 2020

0364-5916/© 2020 Elsevier Ltd. All rights reserved.

**Table 1**  
Thermodynamic parameters used to calculate the Ag–Cu nanosized diagram.

| Variables                | Equations   | Reference |
|--------------------------|---|-----------|
| Surface tension          | $\sigma_{Ag}^{solid} = 1.675 - 0.47 \times 10^{-3} \times T$  | [53]      |
|                          | $\sigma_{Ag}^{liquid} = 1.207 - 2.28 \times 10^{-4} \times T$   | [54]      |
|                          | $\sigma_{Cu}^{solid} = 2.158512 - 4.0 \times 10^{-4} \times T$  | [55]      |
|                          | $\sigma_{Cu}^{liquid} = 1.5834 - 1.8012 \times 10^{-4} \times T$  | [56]      |
| Molar volume             | $V_{Ag}^{solid} = 1.12066 \times 10^{-5}$   | [28]      |
|                          | $V_{Ag}^{liquid} = 1.0198 \times 10^{-5} + 1.1368 \times 10^{-9} \times T$  | [28]      |
|                          | $V_{Cu}^{solid} = 7.01 \times 10^{-6} + 2.92 \times 10^{-10} \times T + 1.02 \times 10^{-13} \times T^2$  | [52]      |
|                          | $V_{Cu}^{liquid} = 7.53 \times 10^{-6} + 2.49 \times 10^{-10} \times T + 1.86 \times 10^{-13} \times T^2$   | [52]      |
| Excess molar free energy | $G_{Liquid}^{Ex} = X_{Ag}X_{Cu}[(17534.6 - 4.45479 \times T) + (2251.3 - 2.6733 \times T) \times (X_{Ag} - X_{Cu}) + 492.7 \times (X_{Ag} - X_{Cu})^2]$ | [53]      |
|                          | $G_{Solid}^{Ex} = X_{Ag}X_{Cu}[(33819.1 - 8.1236 \times T) + (-5601.9 + 1.32997 \times T) \times (X_{Ag} - X_{Cu})]$                                    | [53]      |

respectively. Their results showed relatively large differences of melting temperature compared with the work by Hajra and Acharya [34], due to lack of experimental data on the melting behavior of pure Ag, Cu, and Ag–Cu NPs. Sopoušek et al. [41] experimentally and thermodynamically investigated the melting behavior and phase diagram of Ag–Cu nanoalloy with size of 20 nm. However, as discussed by Sopoušek et al. themselves, the calculated eutectic melting temperature depression was not observed experimentally. However, only about 14 K melting point depression of Ag–Cu nanoalloys with the size of 10 nm was reported by Delsante et al. [42], not be used to compare with the calculated results in this work, due to a side-segregated configuration. Using modified

CALPHAD type thermodynamic model, Jabbareh and Monji [43] reassessed the phase diagram of Ag–Cu nanoalloy. The surface energy of liquid Ag–Cu NPs with different sizes and the phase diagrams of Ag–Cu NPs with the radius of 10 nm and 2 nm, together with the bulk Ag–Cu phase diagram, were calculated respectively. Due to lack of experimental data, only the calculated solid solubility was compared with the results calculated by Monte Carlo method [44]. Recently, Su et al. [37] experimentally investigated the size-dependent melting behavior of four silica-coated Ag–Cu NPs with the radius of 5.25 nm, 4.60 nm, 4.45 nm and 4.25 nm, respectively. Nonlinear size-dependent melting behavior was found for Ag–Cu NPs encapsulated in silica. Consequently, although several works on the phase diagram of Ag–Cu NPs at nanoscale have been reported [34,40,41,43], large discrepancy on the theoretical and experimental melting behavior and phase diagram exists in the Ag–Cu system at nanoscale, due to lack of experimental data on the melting of Ag–Cu NPs or experimental data not be considered. The objective of this work is to thermodynamically reassess the phase diagram of Ag–Cu system at nanoscale to obtain the self-consistent and reliable thermodynamic parameters, mainly on the basis of our previous studies on the melting behavior of Ag [35] and Ag–Cu [37] NPs.

## 2. Thermodynamic modeling

Different methods have been employed to calculate the Gibbs energy for nanoalloys. For the size larger than about 5 nm, it is shown that thermodynamic modeling plays an effective role which can correctly predict the melting points and equilibria for NPs [25]. For the system of Ag–Cu NPs, the total Gibbs free energy comprises the Gibbs free energy of the surface and the bulk.

$$G^{Total} = G^{Bulk} + G^{Surface} \quad (1)$$

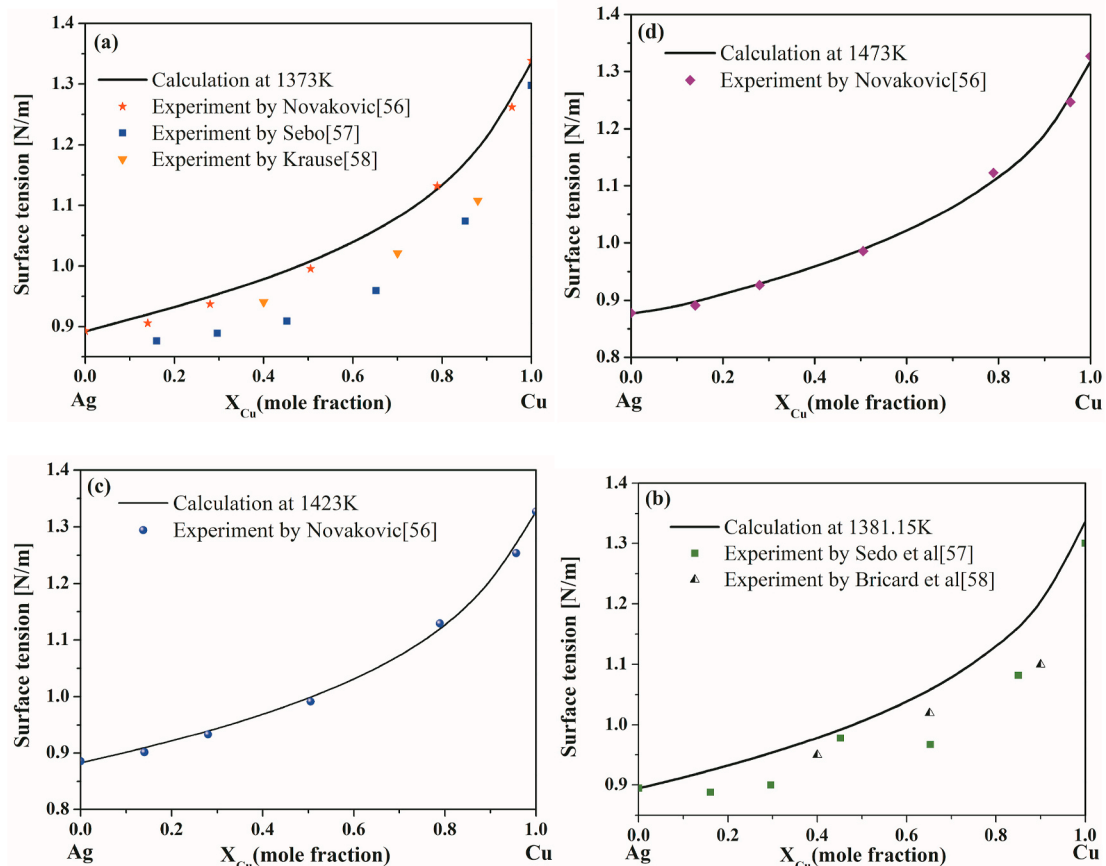


**Fig. 1.** Calculated surface tensions of Ag–Cu alloy of solid phase as a function of Cu composition for various temperatures compared with experimental data.

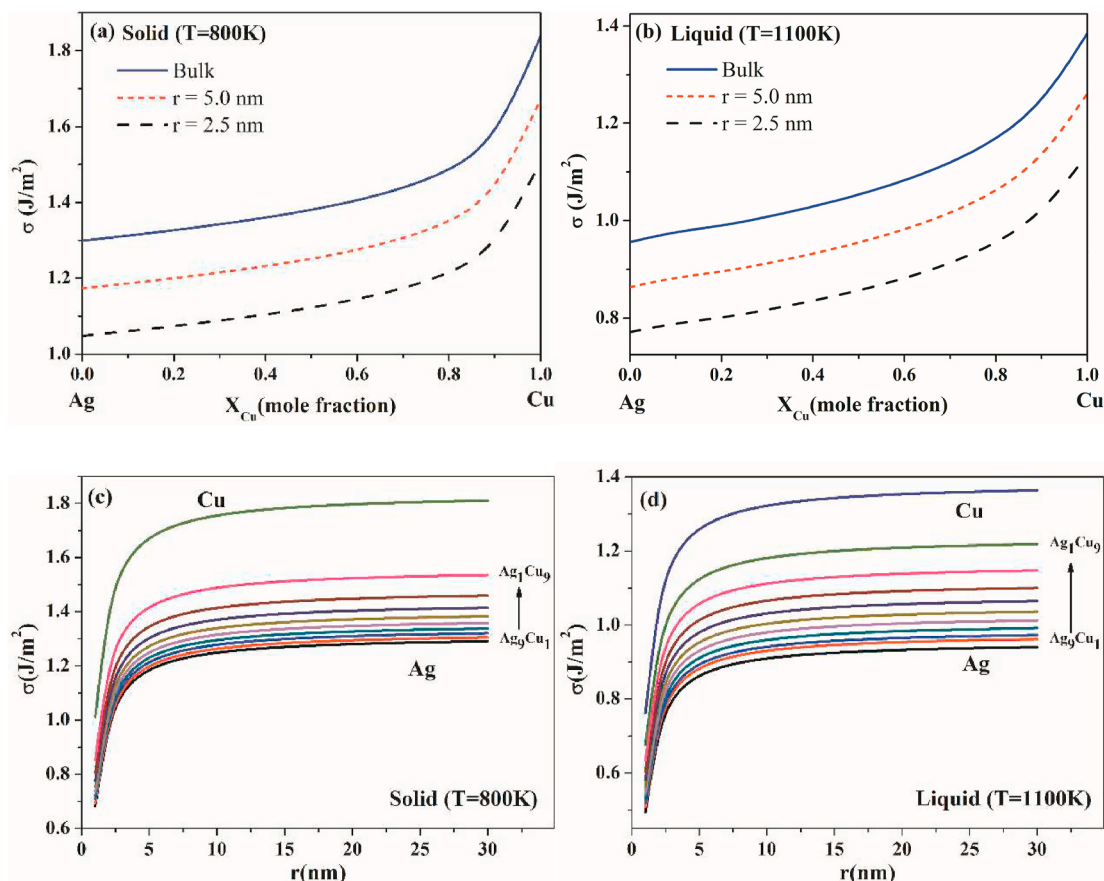


Fig. 2. Calculated the surface energies with various radii compared with the bulk (a) solid phase at T = 800 K, (b) liquid phase at T = 1100 K, and surface energies with various compositions from pure Ag, Cu and Ag–Cu NPs, (c) solid phase at T = 800 K, (d) liquid phase at T = 1100 K, respectively.

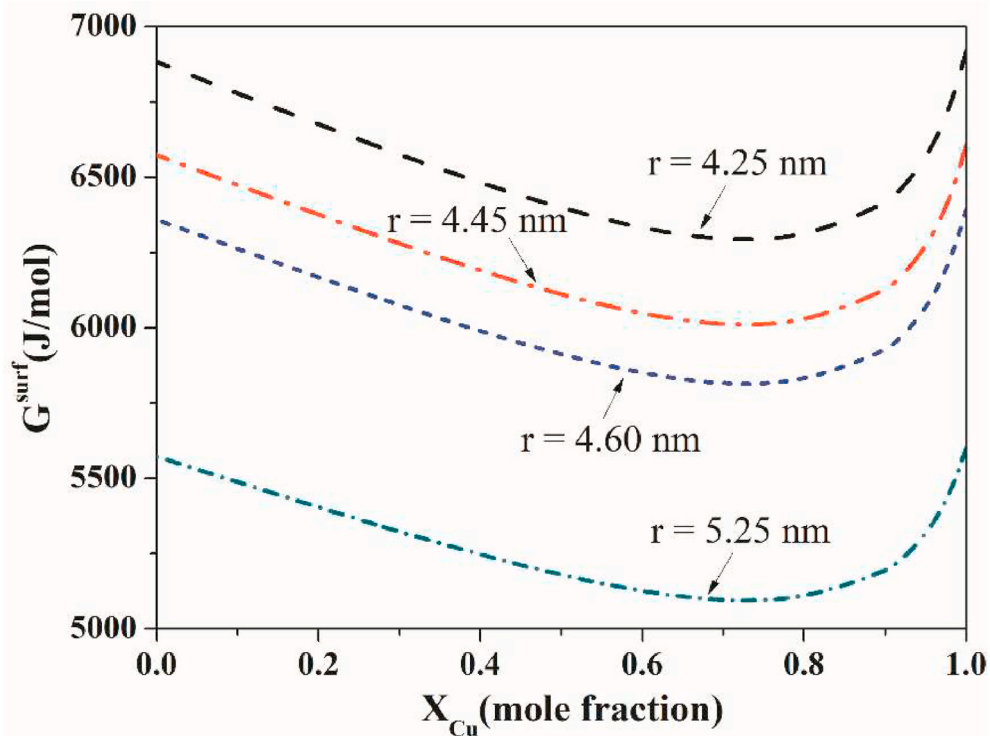


Fig. 3. Calculated Gibbs free energy contributed by surface effect of Ag–Cu NPs for liquid phase with different particle sizes at 1100 K.

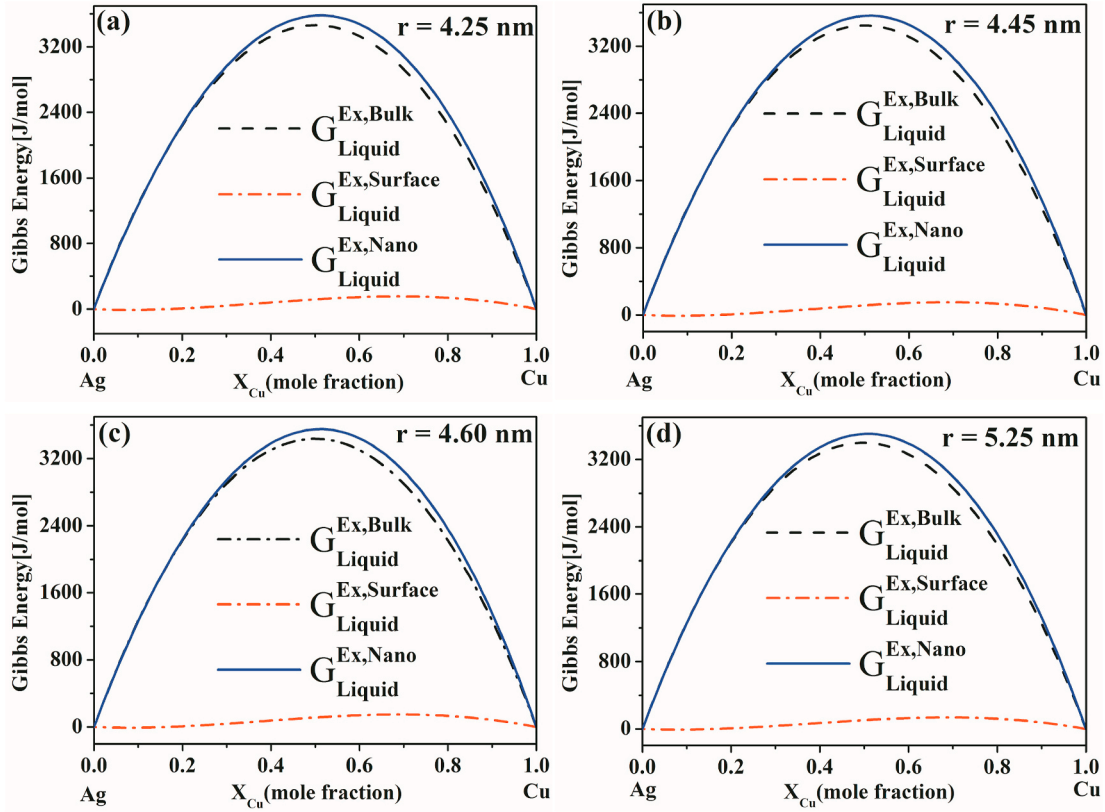


Fig. 4. Nano and bulk contributions to the excess Gibbs energy (a)  $r = 4.25$  nm; (b)  $r = 4.45$  nm; (c)  $r = 4.60$  nm; (d)  $r = 5.25$  nm, respectively.

The molar Gibbs energy for the bulk is defined as

$$G^{Bulk} = X_{Ag}G_{Ag}^0 + X_{Cu}G_{Cu}^0 + RT(X_{Ag}\ln X_{Ag} + X_{Cu}\ln X_{Cu}) + G^{Ex,Bulk} \quad (2)$$

where  $X_{Ag}$  and  $X_{Cu}$  represent the mole fractions,  $G_{Cu}^0$  and  $G_{Ag}^0$  represent the standard Gibbs free energy for pure components of the binary system, respectively. Here the  $R$  represents the gas constant and the value is 8.314, and the parameter  $T$  represents the absolute temperature for alloy. For the bulk of binary system,  $G_{AgCu}^{Ex}$  represent the excess Gibbs free energy. It can be described by the Redlich-Kister polynomial [45].

$$G_{AgCu}^{Ex} = X_{Ag}X_{Cu} \sum L^v (X_{Ag} - X_{Cu})^v \quad (v=0, 1, 2, \dots) \quad (3)$$

$L^v$  represents the interaction parameter which is defined as Eq. (4)

$$L^v = a + bT + cT\ln(T) + \dots \quad (4)$$

The molar surface Gibbs free energy for Ag–Cu NPs can be expressed as:

$$G^{Surface} = 2C\sigma_{AgCu}V_{AgCu}/r \quad (5)$$

where  $\sigma_{AgCu}$  and  $V_{AgCu}$  represent the surface tension and molar volume of Ag–Cu NPs, respectively. The parameter  $r$  represents the particles' radius. For the isotropic spherical particles, the correction factor  $C$  was determined by optimizing and fitting the experimental data considering the shape effect and surface tension. Here, the molar volume for binary system of Ag–Cu NPs consists of the sum of fraction in two components.

$$V = X_{Ag}V_{Ag} + X_{Cu}V_{Cu} \quad (6)$$

where  $V_{Ag}$  and  $V_{Cu}$  are the molar volume for different components of the binary system. For Ag–Cu system, the surface tension of binary system was calculated by Butler's equation [46].

$$\begin{aligned} \sigma_{AgCu} &= \sigma_{Ag} + \frac{RT}{A_{Ag}} \ln \left( \frac{X_{Ag}^{Surface}}{X_{Ag}^{Bulk}} \right) \\ &+ \frac{A_{Ag}}{A_{Cu}} \left[ G_{Ag}^{Ex,Surface}(T, X_{Ag}^{Surface}) - G_{Ag}^{Ex,Bulk}(T, X_{Ag}^{Bulk}) \right] \\ &= \sigma_{Cu} + \frac{RT}{A_{Cu}} \ln \left( \frac{X_{Cu}^{Surface}}{X_{Cu}^{Bulk}} \right) \\ &+ \frac{A_{Cu}}{A_{Ag}} \left[ G_{Cu}^{Ex,Surface}(T, X_{Cu}^{Surface}) - G_{Cu}^{Ex,Bulk}(T, X_{Cu}^{Bulk}) \right] \end{aligned} \quad (7)$$

where  $A_{Ag}$  and  $A_{Cu}$  are the molar surface area for different components of the binary system combined with molar volume data and the Avogadro's number.  $G_{Ag}^{Ex,Surface}(T, X_{Ag}^{Surface})$ ,  $G_{Cu}^{Ex,Surface}(T, X_{Cu}^{Surface})$ ,  $G_{Ag}^{Ex,Bulk}(T, X_{Ag}^{Bulk})$  and  $G_{Cu}^{Ex,Bulk}(T, X_{Cu}^{Bulk})$  are the excess Gibbs free energy of the corresponding component relative to the surface and bulk phase, respectively.

Eq. (8) is to calculate the molar surface area

$$A_i = 1.091N_0^{1/3}V_0^{2/3} \quad (8)$$

According to Yeum's [47] model and Tanaka's [48] viewpoint, the relationship between surface and bulk excess energy is shown as

$$G_{Ag}^{Ex,Surface}(T, X_{Ag}^{Surface}) = \beta^{Mix} G_{Ag}^{Ex,Bulk}(T, X_{Ag}^{Bulk}) \quad (9)$$

where  $\beta$  is expressed by the ratio of the coordination numbers of the surface and bulk phase and indicates reduced coordination. According to the literature [49], the value of  $\beta$  in the liquid phase is 0.85, and the value of  $\beta$  in the solid phase is 0.84. Here the  $G_{Ag}^{Ex,Bulk}$  is given by Eq. (10), the same equation for component Cu.

$$G_{Ag}^{Ex,Bulk} = G_{AgCu}^{Ex} + (1 - X_{Ag})dG_{AgCu}^{Ex} / dX_{Ag} \quad (10)$$

From a thermodynamic viewpoint, when the surface effect of the NPs was considered, the Gibbs energy per molar Ag–Cu NPs could be expressed as

**Table 2**

The reassessed Gibbs energies of Ag, Cu at nanoscale and modified interaction parameters of the liquid and solid phase.

| Silver                          |   |
|---------------------------------|---|
| Between 298.15 and 1235.08 K    |   |
| $G_{Ag}^{0,solid}$              | $= -7209.512 + \frac{4.7491 \times 10^{-5}}{r} + \left(118.200733 - \frac{1.33258 \times 10^{-8}}{r}\right) * T - 23.84633 * T \ln(T) - 0.001790585 * T^2 - 3.98587 * 10^{-7} * T^3 - 12011 * T^{-1}$   |
| $G_{Ag}^{0,liquid}$             | $= 3815.781 + \frac{2.4618 \times 10^{-5}}{r} + \left(109.310587 - \frac{1.90606 \times 10^{-9}}{r}\right) * T - 23.8463314 * T \ln(T) - \left(0.001790585 + \frac{5.1838 \times 10^{-13}}{r}\right) * T^2 - 3.98587 * 10^{-7} * T^3 - 12011 * T^{-1} - 1.0322 * 10^{-20} * T^7$  |
| Between 1235.08 K and 3000.00 K |   |
| $G_{Ag}^{0,solid}$              | $= -15095.314 + \frac{4.7491 \times 10^{-5}}{r} + \left(190.265169 - \frac{1.33258 \times 10^{-8}}{r}\right) * T - 33.472 * T \ln(T) - 1.412186 \times 10^{29} * T^{-9}$  |
| $G_{Ag}^{0,liquid}$             | $= -3587.342 + \frac{2.4618 \times 10^{-5}}{r} + \left(180.964674 - \frac{1.90606 \times 10^{-9}}{r}\right) * T - 33.472 * T \ln(T) - \frac{5.1838 \times 10^{-13}}{r} * T^2$   |
| Copper                          |   |
| Between 298.15 and 1358.02 K    |   |
| $G_{Cu}^{0,solid}$              | $= -7770.458 + \frac{3.0457 \times 10^{-5}}{r} + \left(130.485403 - \frac{4.37539 \times 10^{-9}}{r}\right) * T - 24.112392 * T \ln(T) - \left(0.00265684 - \frac{2.08066 \times 10^{-13}}{r}\right) * T^2 + \left(1.29223 \times 10^{-7} - \frac{8.21245 \times 10^{-17}}{r}\right) * T^3 + 52478 * T^{-1}$  |
| $G_{Cu}^{0,liquid}$             | $= 5194.382 + \frac{2.3846 \times 10^{-5}}{r} + \left(120.97516 - \frac{1.92408 \times 10^{-9}}{r}\right) * T - 24.112392 * T \ln(T) - \left(0.00265684 - \frac{4.99325 \times 10^{-13}}{r}\right) * T^2 + \left(1.29223 \times 10^{-7} + \frac{6.70045 \times 10^{-17}}{r}\right) * T^3 + 52478 * T^{-1} - 5.83932 \times 10^{-21} * T^7$  |
| Between 1358.02 K and 3200.00 K |   |
| $G_{Cu}^{0,solid}$              | $= -13542.33 + \frac{3.0457 \times 10^{-5}}{r} + \left(183.804197 - \frac{4.37539 \times 10^{-9}}{r}\right) * T - 31.38 * T \ln(T) + 3.64643 \times 10^{29} * T^{-9} + \frac{2.08066 \times 10^{-13}}{r} * T^2 - \frac{8.21245 \times 10^{-17}}{r} * T^3$   |
| $G_{Cu}^{0,liquid}$             | $= -46.93 + \frac{2.3981 \times 10^{-5}}{r} + \left(173.883734 - \frac{1.92408 \times 10^{-9}}{r}\right) * T - 31.38 * T \ln(T) + \frac{4.99325 \times 10^{-13}}{r} * T^2 - \frac{6.70045 \times 10^{-17}}{r} * T^3$  |
| Excess Gibbs Energy             |   |
| $G_{Liquid}^{Ex, Nano}$         | $= X_{Ag} X_{Cu} \left\{ \left(17534.6 - \frac{8.935 \times 10^{-6}}{r}\right) + \left(-4.45479 + \frac{4.244 \times 10^{-9}}{r}\right) * T + \left[2251.3 - \frac{6.2246 \times 10^{-7}}{r} + \left(-2.6733 + \frac{4.6545 \times 10^{-9}}{r}\right) * T\right] * (X_{Ag} - X_{Cu}) + \left(492.7 - \frac{2.9635 \times 10^{-8}}{r}\right) * (X_{Ag} - X_{Cu})^2 \right\}$   |
| $G_{Solid}^{Ex, Nano}$          | $= X_{Ag} X_{Cu} \left\{ \left(33819.1 - \frac{C^* 1.718 \times 10^{-6}}{r}\right) + \left(-8.1236 - \frac{C^* 1.78425 \times 10^{-10}}{r}\right) * T + \left[-5601.9 + \frac{C^* 4.2966 \times 10^{-7}}{r} + \left(1.32997 + \frac{C^* 6.888 \times 10^{-9}}{r}\right) * T\right] * (X_{Ag} - X_{Cu}) + \left(\frac{C^* 1.718 \times 10^{-6}}{r} + \frac{C^* 9.7705 \times 10^{-10}}{r} * T\right) * (X_{Ag} - X_{Cu})^2 \right\}$ |

$$G_{AgCu}^{Nano} = G_{AgCu}^{bulk} + 2C\sigma_{AgCu} V_{AgCu} / r \quad (11)$$

By the Redlich-Kister polynomials, excess Gibbs energy for NPs is given by Eq. (12)

$$G^{Ex, Nano} = X_{Ag} X_{Cu} \sum L^v (X_{Cu} - X_{Ag})^v \quad (v=0, 1, 2, \dots) \quad (12)$$

$$\begin{aligned} L^{v, Nano} &= L^{Bulk} + L^{Surface} = f_1 \left(\frac{1}{\gamma}\right) + f_2 \left(\frac{1}{\gamma}\right) T + f_3 \left(\frac{1}{\gamma}\right) T \ln(T) + \dots \\ &= \left(a + \frac{a'}{\gamma}\right) + \left(b + \frac{b'}{\gamma}\right) T + \left(c + \frac{c'}{\gamma}\right) T \ln(T) + \dots \end{aligned} \quad (13)$$

the parameters  $a$ ,  $b$ , and  $c$  in Eq. (13) are in common with the bulk in Eq. (4),  $a'$ ,  $b'$ ,  $c'$  and ... are given by

$$a' + b'T + c'T \ln(T) + \dots = 2C(\sigma_{alloy} V_{alloy} - X_{Ag} \sigma_{Ag} V_{Ag} - X_{Cu} \sigma_{Cu} V_{Cu}) \quad (14)$$

The surface energy for spherical NPs is written as [50].

$$\sigma = \sigma_{AB} (1 - 2\delta_{AB} / r) \quad (15)$$

where  $\sigma$  represents the surface energy of nanoalloy, and the  $\delta_{AB}$  is the constant of bulk which determined by Eq. (16)

$$\delta_{AB} = X_A \delta_A + X_B \delta_B \quad (16)$$

the values of  $\delta_A$  and  $\delta_B$  are 0.2415 and 0.225 for Ag and Cu, respectively, determined by Nanda's work [50].

Take the surface effect into the total Gibbs free energy on basis of above model which is related to temperature, composition, and particle size. And the particle size as a variable impact on the total Gibbs free energy caused the phase equilibrium temperatures deviations.

### 3. Results and discussion

In this work, the thermodynamic description of the Ag-Cu system [51] and the corresponding thermodynamic parameters of the bulk were used as input for the calculations of its phase diagram at nanoscale. The thermodynamic properties of pure components are obtained from the reported in literature [35,52]. The values of correction factor of  $C_{Ag}$  and  $C_{Cu}$  are evaluated to be 1.265 and 1.006, respectively. By fitting experimental melting temperature of Ag-Cu NPs, the correction factor  $C_{Ag-Cu}$  was determined to be 1.305 [37]. According to the above thermodynamic model, the thermodynamic optimization of the Ag-Cu nano system was performed by considering the reported melting results of Ag, Cu and Ag-Cu NPs. A self-consistent thermodynamic data set for the Ag-Cu nano system was obtained and summarized in Table 1. Four nanophase diagrams of Ag-Cu system with a radius of 4.25 nm, 4.45 nm, 4.60 nm and 5.25 nm were calculated, respectively.

Fig. 1 shows the calculated results of surface tensions for Ag-Cu alloy of solid phase as a function of Cu composition for various temperatures compared with experimental data. It's found from Fig. 1 (a)-(d) that the surface tension increases nonlinearly along with increasing Cu component at various temperatures. The calculated results are in good agreement with the experimental data [56-58]. The calculated surface tensions shown in Fig. 1 (b) in the Ag-Cu alloy system at 1381.15 K agree with the calculated results by Hajra and Acharya [34], and experimental results [57,58]. It shows that Ag is always enriched on the surface of the alloy, observed by Lu et al. [59], when calculating the surface composition by the Bulter's equation. Atoms with lower surface energy as silver tend to concentrate in the surface of alloy to reduce the energy of the system.

Fig. 2 demonstrates the calculated results of surface energies for Ag-Cu NPs with various radii and compositions under the condition of solid phase at 800 K and liquid phase at 1100 K, respectively. As shown in Fig. 2(a) and (b), the surface energy of Ag-Cu alloys increases nonlinearly with the increase of particle size and the content of Cu component for both solid and liquid phase. Fig. 2(c) and (d) indicate that Ag has lower energy compared with Cu, which explains the phenomenon of Ag is always enriched on the surface of the alloy and the value of surface energy decreased significantly with the radius below 10 nm. These findings agree with the results reported by Jabbareh and Monji [43].

Fig. 3 reveals that calculated Gibbs free energy contributed by the surface effect of Ag-Cu NPs for liquid phase with different radius of 4.25 nm, 4.45 nm, 4.60 nm, 5.25 nm at 1100 K, respectively. It is revealed that the Gibbs free energy contributed by the surface effect increases with the decreasing particle size, due to an increasing proportion of the total Gibbs free energy. This tendency on the Gibbs free energy

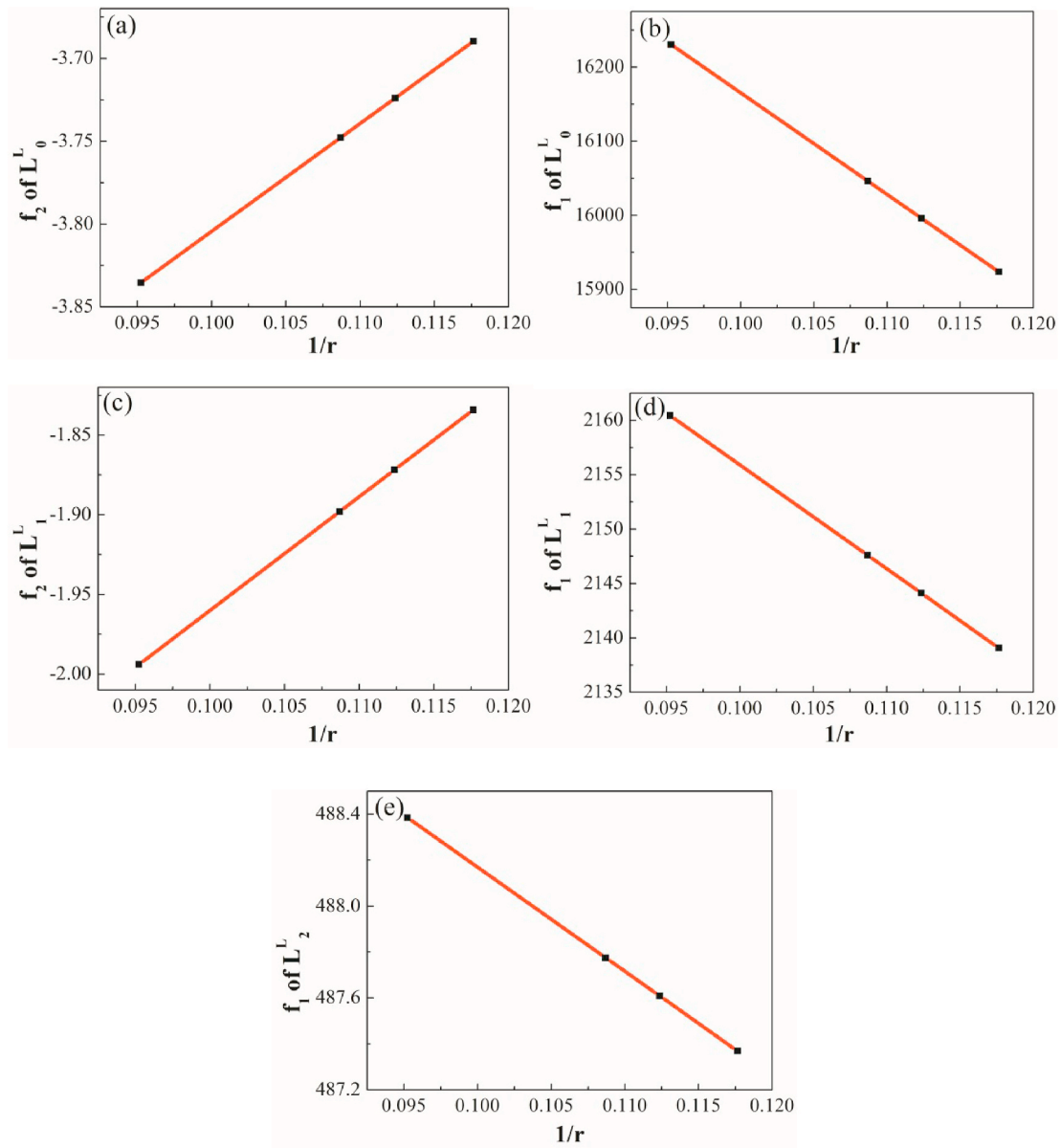


Fig. 5. The relationship between  $f_1, f_2$  of  $L_v$  ( $v = 0, 1, 2$ ) and  $1/r$  for liquid Ag–Cu nanoalloys.

contribution by the surface effect has also been reported by Jabbareh and Monji [43]. This finding can be used to interpret the experimental melting temperature depression of Ag–Cu NPs [37].

Fig. 4 shows that the calculated excess Gibbs energy with the radius of 4.25 nm, 4.45 nm, 4.60 nm, 5.25 nm, reported in previous work [37], respectively. The excess Gibbs energy for liquid alloys is determined by a set of parameters  $L_v^{Surface}$ . The surface tension and molar volume of corresponding component and the excess molar free energy of Ag–Cu alloys are shown in Table 1, and the thermodynamic parameters for Ag–Cu alloys were derived from the modified thermodynamic optimization [53] listed in Table 2. The thermodynamic parameters were obtained by the Scientific Group Thermodata Europe (SGTE) database [60] for bulk Ag and Cu, respectively.

Fig. 5 and Fig. 6 show that the relationship between  $f_1, f_2$  of  $L_v$  ( $v = 0, 1, 2$ ) and reciprocal of radius for liquid and solid Ag–Cu NPs, respectively. According to the excess molar free energy of the Ag–Cu alloy in Table 1, the data of  $L_v$  of Ag–Cu NPs was obtained by Eqs. (3) and (7). The parameters of  $L_0^L, L_1^L, L_2^L, L_0^S, L_1^S$  and  $L_2^S$  could be written with respect to melting temperature and particle size and the polynomials are listed as

Eqs. (17) and (18). The excellent linear relationship proves the reliability of the calculated results.

$$\begin{aligned}
 L_0^{Nano,L} &= \left( 17534.6 - \frac{8.935 \cdot 10^{-6}}{r} \right) + \left( -4.45479 + \frac{4.244 \cdot 10^{-9}}{r} \right) * T \\
 L_1^{Nano,L} &= \left( 2251.3 - \frac{6.2246 \cdot 10^{-7}}{r} \right) + \left( -2.6733 + \frac{4.65465 \cdot 10^{-9}}{r} \right) * T \\
 L_2^{Nano,L} &= 492.7 - \frac{2.95635 \cdot 10^{-8}}{r}
 \end{aligned} \tag{17}$$

$$\begin{aligned}
 L_0^{Nano,S} &= \left( 33819.1 - \frac{1.718 \cdot 10^{-6}}{r} \right) + \left( -8.1236 - \frac{1.78425 \cdot 10^{-10}}{r} \right) * T \\
 L_1^{Nano,S} &= \left( -5601.9 + \frac{4.2966 \cdot 10^{-7}}{r} \right) + \left( 1.32997 + \frac{6.883 \cdot 10^{-9}}{r} \right) * T \\
 L_2^{Nano,S} &= \frac{1.718 \cdot 10^{-6}}{r} + \frac{9.7705 \cdot 10^{-10}}{r} * T
 \end{aligned} \tag{18}$$

Fig. 7 reveals the calculated enthalpy of mixing of liquid phase of Ag–Cu bulk and Ag–Cu nano system with different radius. It is seen that enthalpy of mixing of liquid of Ag–Cu nanoalloys increase with the

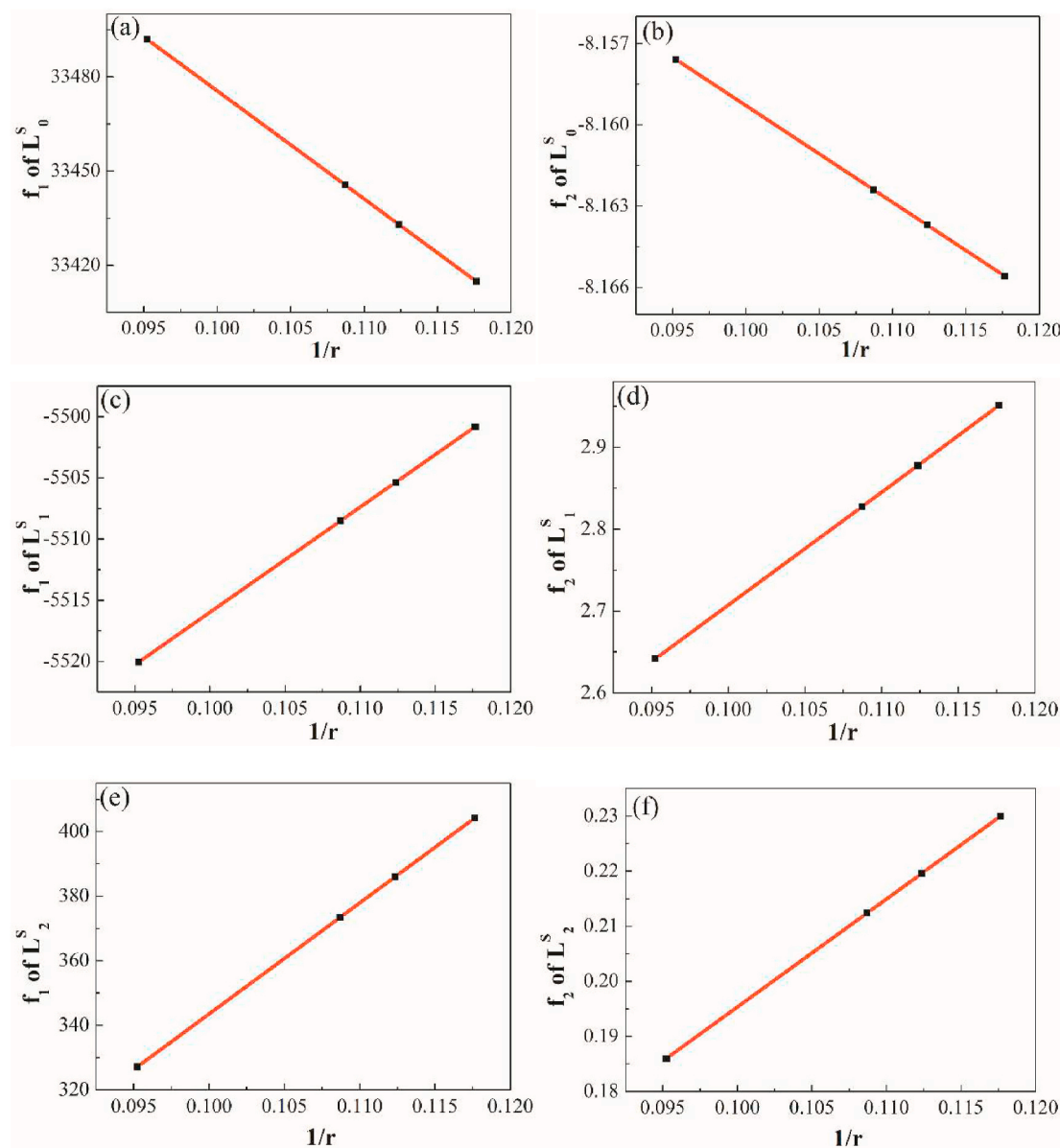


Fig. 6. The relationship between  $f_1$ ,  $f_2$  of  $L_v$  ( $v = 0, 1, 2$ ) and  $1/r$  for solid Ag-Cu nanoalloys.

increase of the radius. Additionally, it is found that the calculated enthalpies of mixing of liquid phase of Ag-Cu bulk alloys are in good agreement with the reported experimental data [61].

Finally, based on the obtained thermodynamic parameters in this work, the phase diagrams of Ag-Cu nanoalloys with a radius of 4.25 nm, 4.45 nm, 4.60 nm and 5.25 nm, as well as Ag-Cu bulk alloy, were calculated, respectively. Fig. 8 (a) shows the calculated phase diagrams of Ag-Cu system with various radii at nanoscale together with the phase diagram for the bulk and experimental data. The calculated melting temperatures of pure Ag, Cu, and Ag-Cu NPs, along with experimental data, are shown in Fig. 8 (b). It is found that the decreasing of liquidus, solidus and eutectic temperature, by decreasing the particle size, was also reported in literature [34,40,41,43]. Furthermore, since the present thermodynamic assessment is performed on the basis of the experimental melting behavior of Ag [35], Cu [36] and Ag-Cu [37], it is clearly shown that the calculated nano phase diagrams of Ag-Cu system at nanoscale are in good agreement with the experimental data on the melting of Ag [35], Cu [36] and Ag-Cu NPs [37], except for Ag-Cu NPs [38]. Additionally, it is clearly shown that the calculated depression values are larger than that reported calculated [34,40,41,43] and

experimental results [38,42] in literature. Consequently, compared with previous calculation in literature, better agreement with experimental results has been obtained.

#### 4. Conclusions

The Ag-Cu phase diagram at nanoscale has been re-investigated via thermodynamic modeling, considering the surface effect on the chemical potential of pure substance and excess Gibbs free energy of mixtures. A self-consistent set of thermodynamic parameters has been obtained by considering the reported melting behavior of Ag, Cu, and Ag-Cu NPs. The calculated phase diagrams agree well with the experimental data.

#### Data availability

The raw/processed data required to reproduce these findings are available to download from [<https://doi.org/10.17632/b9p6x2mvtp.1>].

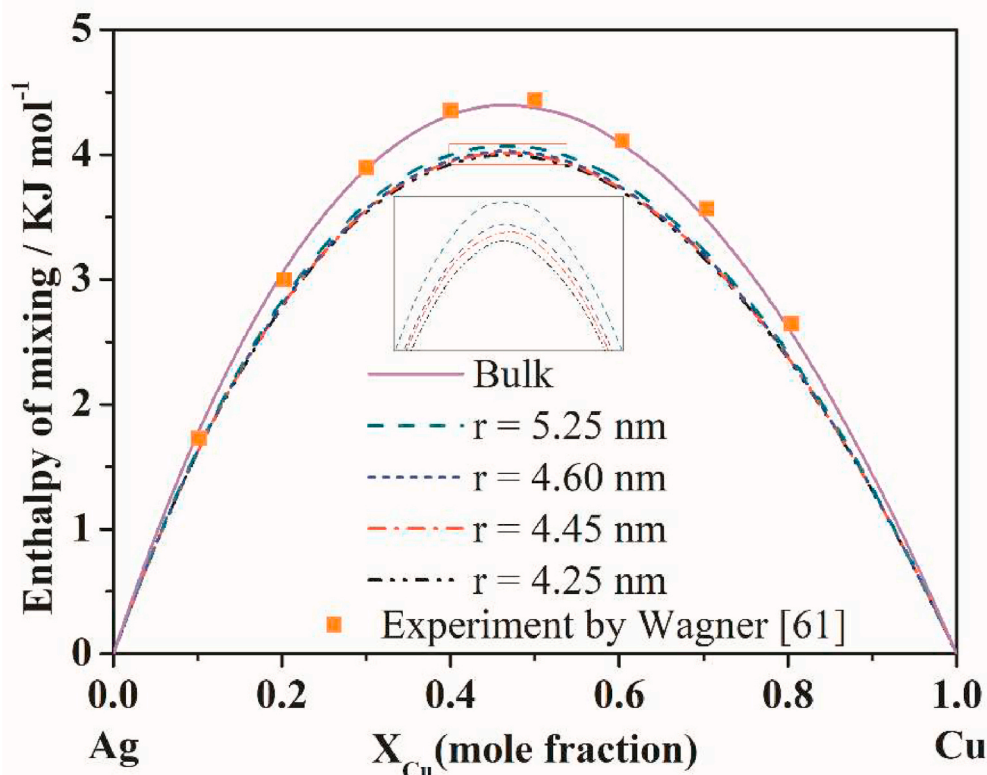


Fig. 7. Enthalpy of mixing of liquid Ag–Cu NPs with radius from 4.25 nm to 5.25 nm [37], respectively, compared with the bulk alloys [61].

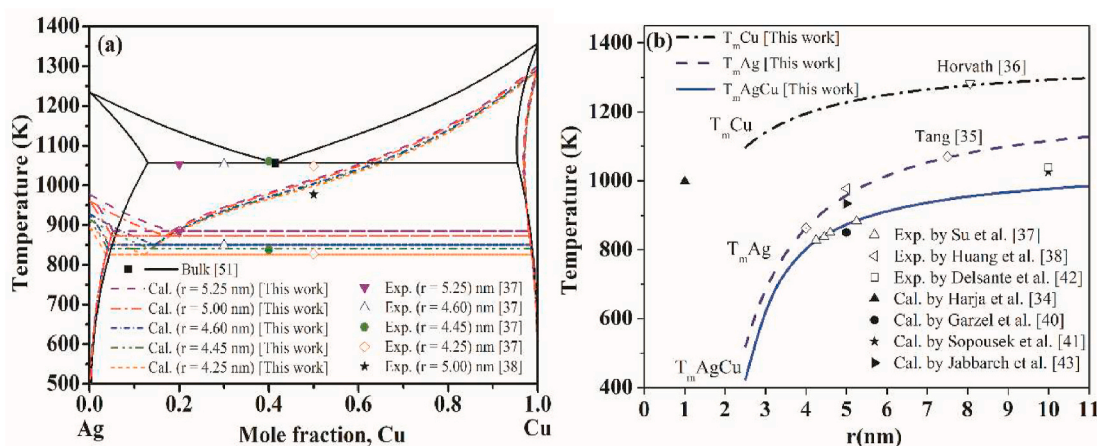


Fig. 8. Reassessed phase diagram of Ag–Cu NPs with different radius (a) and melting temperatures of pure Ag, Cu and Ag–Cu NPs (b) along with experimental results.

#### Declaration of competing interest

The authors declare that there is no conflict of interests regarding the publication of this paper.

#### Acknowledgements

This work was financially supported by the National Natural Science Foundation of China (51761005), the Guangxi Natural Science Foundation (2019GXNSFAA245004, 2016GXNSFGA380001), GUET Excellent Graduate Thesis Program (18YJPYSS29) and Innovation Project of GUET Graduate Education (2020YCX117).

#### Appendix A. Supplementary data

Supplementary data to this article can be found online at <https://doi.org/10.1016/j.calphad.2020.102233>.

#### References

- [1] S. Kwon, W.K. Choi, Understanding the unique electronic properties of nano structures using photoemission theory, *Sci. Rep.* 5 (2015) 17834, <https://doi.org/10.1038/srep17834>.
- [2] C. Di Paola, R. D'Agosta, F. Baletto, Geometrical effects on the magnetic properties of nanoparticles, *Nano Lett.* 16 (2016) 2885–2889, <https://doi.org/10.1021/acs.nanolett.6b00916>.
- [3] F. Yang, D. Deng, X. Pan, Q. Fu, X. Bao, Understanding nano effects in catalysis, *Natl. Sci. Rev.* 2 (2015) 183–201, <https://doi.org/10.1093/nsr/nwv024>.

- [4] Z. Zhang, J.C. Li, Q. Jiang, Modelling for size-dependent and dimension-dependent melting of nanocrystals, *J. Phys. D Appl. Phys.* 33 (2000) 2653–2656, <https://doi.org/10.1088/0022-3727/33/20/318>.
- [5] K.K. Nanda, Size-dependent melting of nanoparticles: hundred years of thermodynamic model, *Pramana* 72 (4) (2009) 617–628, <https://doi.org/10.1007/s12043-009-0055-2>.
- [6] F. Calvo, Thermodynamics of nanoalloys, *Phys. Chem. Chem. Phys.* 17 (2015) 27922, <https://doi.org/10.1039/c5cp00274e>.
- [7] K. Brandner, K. Saito, U. Seifert, Thermodynamics of micro- and nano-systems driven by periodic temperature variations, *Phys. Rev. X* 5 (3) (2015), 031019, <https://doi.org/10.1103/physrevx.5.031019>.
- [8] J. Lee, T. Tanaka, H. Mori, K. Penttilä, Phase diagrams of nanometer-sized particles in binary systems, *JOM (J. Occup. Med.)* 57 (2005) 56–59, <https://doi.org/10.1007/s11837-005-0235-6>.
- [9] E. Sutter, P. Sutter, Phase diagram of nanoscale alloy particles used for vapor-liquid-solid growth of semiconductor nanowires, *Nano Lett.* 8 (2008) 411–414, <https://doi.org/10.1021/nl0719630>.
- [10] S. Xiong, W. Qi, B. Huang, M. Wang, Z. Li, S. Liang, Size-temperature phase diagram of titanium nanosolids, *J. Phys. Chem. C* 116 (2012) 237–241, <https://doi.org/10.1021/jp208149d>.
- [11] Z. Zhang, M. Zhao, Q. Jiang, Melting temperatures of semiconductor nanocrystals in the mesoscopic size range, *Semicond. Sci. Technol.* 16 (2001) L33–L35, <https://doi.org/10.1088/0268-1242/16/6/101>.
- [12] C.Q. Sun, Y. Wang, B.K. Tay, S. Li, H. Huang, Y.B. Zhang, Correlation between the melting point of a nanosolid and the cohesive energy of a surface atom, *J. Phys. Chem. B* 106 (2002) 10701–10705, <https://doi.org/10.1021/jp025868l>.
- [13] Z. Zhang, J.C. Li, Q. Jiang, Modelling for size-dependent and dimension-dependent melting of nanocrystals, *J. Phys. D Appl. Phys.* 33 (2000) 2653–2656, <https://doi.org/10.1088/0022-3727/33/20/318>.
- [14] A. Safaei, M. Attarian Shandiz, S. Sanjabi, Z.H. Barber, Modelling the size effect on the melting temperature of nanoparticles, nanowires and nanofilms, *J. Phys. Condens. Matter* 19 (2007) 216216, <https://doi.org/10.1088/0953-8984/19/21/216216>.
- [15] Grégory Guisbiers, Advances in thermodynamic modelling of nanoparticles, *Adv. Phys. X* 4 (2019) 1, <https://doi.org/10.1080/23746149.2019.1668299>, 1668299.
- [16] S. Xiao, W. Hu, J. Yang, Melting behaviors of nanocrystalline Ag, *J. Phys. Chem. B* 109 (2005) 20339–20342, <https://doi.org/10.1021/jp054551t>.
- [17] Z.M. Ao, W.T. Zheng, Q. Jiang, Size effects on the Kauzmann temperature and related thermodynamic parameters of Ag nanoparticles, *Nanotechnology* 18 (2007) 255706, <https://doi.org/10.1088/0957-4484/18/25/255706>.
- [18] Y.J. Li, W.H. Qi, B.Y. Huang, M.P. Wang, S.Y. Xiong, Modeling the thermodynamic properties of bimetallic nanosolids, *J. Phys. Chem. Solid.* 71 (2010) 810–817, <https://doi.org/10.1016/j.jpcs.2010.02.003>.
- [19] H. Namazi, A. Akrami, R. Haghighi, A. Delaviz, V.V. Kulish, Analysis of the influence of element's entropy on the bulk metallic glass (BMG) entropy, complexity, and strength, *Metall. Mater. Trans. B* 48 (2017) 780–788, <https://doi.org/10.1007/s11661-016-3870-3>.
- [20] P. Pawlow, The dependence of the melting point on the surface energy of a solid body, *Z. Phys. Chem.* 65 (1909) 545–548.
- [21] M. Takagi, Electron-diffraction study of liquid-solid transition of thin metal films, *J. Phys. Soc. Jpn.* 9 (1954) 359–363, <https://doi.org/10.1143/JPSJ.9.359>.
- [22] P. Buffat, J.P. Borel, Size effect on the melting temperature of gold particles, *Phys. Rev.* 13 (1976) 2287–2298, <https://doi.org/10.1103/PhysRevA.13.2287>.
- [23] J. Sopotšek, A. Kryštofová, M. Premović, O. Zobač, S. Polsterová, P. Brož, J. Bursík, Au-Ni nanoparticles: phase diagram prediction, synthesis, characterization, and thermal stability, *Calphad* 58 (2017) 25–33, <https://doi.org/10.1016/j.calphad.2017.05.002>.
- [24] M. Zhang, M.Y. Efremov, F. Schiettekatte, E.A. Olson, A.T. Kwan, S.L. Lai, T. Wisleder, J.E. Greene, L.H. Allen, Size-dependent melting point depression of nanostructures: nanocalorimetric measurements, *Phys. Rev. B: Solid State* 62 (2000) 10548–10557, <https://doi.org/10.1103/PhysRevB.62.10548>.
- [25] J. Lee, K.J. Sim, General equations of calphad-type thermodynamic description for metallic nanoparticle systems, *Calphad* 44 (2014) 129–132, <https://doi.org/10.1016/j.calphad.2013.07.008>.
- [26] G. Kaptay, Nano-Calphad: extension of the calphad method to systems with nano-phases and complexions, *J. Mater. Sci.* (2012) 8320–8335, <https://doi.org/10.1007/s10853-012-6772-9>.
- [27] Y. Eichhammer, J. Roeck, N. Moelans, F. Iacopi, B. Blanpain, M. Heyns, Calculation of the Au-Ge phase diagram for nanoparticles, *Arch. Metall. Mater.* 53 (2008) 1133–1139, <https://doi.org/10.9774/GLEAF.978-1-909493-38-4.2>.
- [28] J. Park, J. Lee, Phase diagram reassessment of Ag-Au system including size effect, *Calphad* 32 (2008) 135–141, <https://doi.org/10.1016/j.calphad.2007.07.004>.
- [29] S. Chowdhury, V.R. Bhethanabotla, R. Sen, Effect of Ag-Cu alloy nanoparticle composition on luminescence enhancement/quenching, *J. Phys. Chem. C* 113 (2009) 13016–13022, <https://doi.org/10.1021/jp900294z>.
- [30] K.L. Reddy, S. Kumar, A. Kumar, V. Krishnan, Wide spectrum photocatalytic activity in lanthanide-doped upconversion nanophosphors coated with porous TiO<sub>2</sub> and Ag-Cu bimetallic nanoparticles, *J. Hazard Mater.* 367 (2019) 694–705, <https://doi.org/10.1016/j.jhazmat.2019.01.004>.
- [31] T.L. Chang, X. Zhou, J. Liang, Synthesis and characterization of Ag-Cu alloy nanoparticles for antimicrobial applications: a polydopamine chemistry application, *Mater. Sci. Eng. C* 98 (2019) 675–684, <https://doi.org/10.1016/j.msec.2018.12.092>.
- [32] S.J. Kim, E.A. Stach, C.A. Handwerker, Fabrication of conductive interconnects by Ag migration in Cu-Ag core-shell nanoparticles, *Appl. Phys. Lett.* 96 (2010) 144101, <https://doi.org/10.1063/1.3364132>.
- [33] M.J. Kammer, A. Muza, J. Snyder, A. Rae, S.J. Kim, C.A. Handwerker, Optimization of Cu-Ag core-shell solderless interconnect paste technology, *IEEE Trans. Compon. Packag. Manuf. Technol.* 5 (2015) 910–920, <https://doi.org/10.1109/TCPMT.2015.2438816>.
- [34] J.P. Hajra, S. Acharya, Thermodynamics and phase equilibria involving nano phases in the Cu-Ag system, *J. Nanosci. Nanotechnol.* 4 (2004) 899–906, <https://doi.org/10.1166/jnn.2004.088>.
- [35] C. Tang, Y.M. Sung, J. Lee, Nonlinear size-dependent melting of the silica-encapsulated silver nanoparticles, *Appl. Phys. Lett.* 100 (2012) 201903, <https://doi.org/10.1063/1.4712599>.
- [36] J. Horváth, R. Birringer, H. Gleiter, Diffusion in nanocrystalline material, *Solid State Commun.* 62 (1987) 319–322, [https://doi.org/10.1016/0038-1098\(87\)90989-6](https://doi.org/10.1016/0038-1098(87)90989-6).
- [37] T. Su, H. Xiao, W. Shen, C. Hu, C. Tang, Nonlinear size-dependent melting of silica-encapsulated Ag-Cu alloy nanoparticles, *J. Phys. Chem. C* 122 (2018) 27761–27768, <https://doi.org/10.1021/acs.jpcc.8b09156>.
- [38] C.-H. Huang, H.P. Wang, J.-E. Chang, E.M. Eyring, Synthesis of nanosize-controllable copper and its alloys in carbon shells, *Chem. Commun.* 2 (2009), <https://doi.org/10.1039/b905759e4663-4465>.
- [39] J. Lee, T. Tanaka, J.G. Lee, H. Mori, Effect of substrates on the melting temperature of gold nanoparticles, *Calphad* 31 (2007) 105–111, <https://doi.org/10.1016/j.calphad.2006.10.001>.
- [40] G. Garzel, J. Janczak-Rusch, L. Zabydr, Reassessment of the Ag-Cu phase diagram for nanosystems including particle size and shape effect, *Calphad* 36 (2012) 52–56, <https://doi.org/10.1016/j.calphad.2011.11.005>.
- [41] J. Sopotšek, J. Pinkas, P. Brož, J. Bursík, V. Vykoukal, D. Škoda, A. Stýskalk, O. Zobač, J. Vřešťál, A. Hrdlička, J. Šimbera, Ag-Cu colloid synthesis: bimetallic nanoparticle characterisation and thermal treatment, *J. Nanomater.* 2014 (2014) 13, <https://doi.org/10.1155/2014/638964>.
- [42] S. Delsante, G. Borzone, R. Novakovic, D. Piazza, G. Pigozzi, J. Janczak-Rusch, M. Pilloni, G. Ennas, Synthesis and thermodynamics of Ag-Cu nanoparticles, *Phys. Chem. Chem. Phys.* 17 (2015) 28387–28393, <https://doi.org/10.1039/C5CP02058A>.
- [43] M.A. Jabbareh, F. Monji, Thermodynamic modeling of Ag - Cu nanoalloy phase diagram, *Calphad* 60 (2018) 208–213, <https://doi.org/10.1016/j.calphad.2018.01.004>.
- [44] I. Atanasov, R. Ferrando, L.R. Johnston, Structure and solid solution properties of Cu-Ag nanoalloys, *J. Phys. Condens. Matter* 26 (2014) 275301, <https://doi.org/10.1088/0953-8984/26/27/275301>.
- [45] O. Redlich, A.T. Kister, Algebraic Representation of thermodynamic properties and the classification of solutions, *Ind. Eng. Chem.* 40 (2) (1948) 345–348, <https://doi.org/10.1021/ie50458a036>.
- [46] J.A.V. Butler, The thermodynamics of the surfaces of solutions, *Proc. R. Soc. London, Ser. A* 135 (1932) 348–375, <https://doi.org/10.1098/rspa.1932.0040>.
- [47] K.S. Yeum, R. Speiser, D.R. Poirier, Estimation of the surface tensions of binary liquid alloys, *Metall. Trans. B* 20 (1989) 693–703, <https://doi.org/10.1007/BF02655927>.
- [48] T. Tanaka, K. Hack, S. Hara, Calculation of surface tension of liquid Bi-Sn alloy using thermochemical application library ChemApp, *Calphad* 24 (2000) 465–474, [https://doi.org/10.1016/S0364-5916\(00\)85001-4](https://doi.org/10.1016/S0364-5916(00)85001-4).
- [49] T. Tanaka, K. Hack, T. Iida, S. Hara, Application of thermodynamic databases to the evaluation of surface tensions of molten alloys, salt mixtures and oxide mixtures, *Int. J. Mater. Res.* 87 (1996) 380–389, [https://doi.org/10.1016/1359-6462\(95\)00683-4](https://doi.org/10.1016/1359-6462(95)00683-4).
- [50] K.K. Nanda, Liquid-drop model for the surface energy of nanoparticles, *Phys. Lett.* 376 (2012) 1647–1649, <https://doi.org/10.1016/j.physleta.2012.03.055>.
- [51] F.H. Hayes, H.L. Lukas, G. Effenberg, G. Petzow, Thermodynamic optimization of the Cu-Ag-Pb system, *Met. A.* 77 (1986) 749–754.
- [52] W. Luo, L. Deng, K. Su, K. Li, G. Liao, S. Xiao, Gibbs free energy approach to calculate the thermodynamic properties of copper nanocrystals, *Phys. B Condens. Matter* 406 (2011) 859–863, <https://doi.org/10.1016/j.physb.2010.12.014>.
- [53] J. Lee, M. Nakamoto, T. Tanaka, Thermodynamic study on the melting of nanometer-sized gold particles on graphite substrate, *J. Mater. Sci.* 40 (9–10) (2005) 2167–2171, <https://doi.org/10.1007/s10853-005-1927-6>.
- [54] J. Lee, W. Shimoda, T. Tanaka, Surface tension and its temperature coefficient of liquid Sn-X (X=Ag, Cu) alloys, *Mater. Trans.* 45 (2004) 2864–2870, <https://doi.org/10.2320/matertrans.45.2864-2870>.
- [55] M. Nakamoto, M. Liukkonen, M. Friman, E. Heikinheimo, M. Härmäläinen, L. Holappa, Measurement of surface tension of solid Cu by improved multiphase equilibrium, *Metall. Mater. Trans. B* 39 (2008) 570–580, <https://doi.org/10.1007/s11663-008-9168-0>.
- [56] R. Novakovic, E. Ricci, D. Giuranno, A. Passerone, Surface and transport properties of Ag-Cu liquid alloys, *Surf. Sci.* 576 (2005) 175–187, <https://doi.org/10.1016/j.susc.2004.12.009>.
- [57] P. Sebo, B. Gallois, C.H.P. The surface tension of liquid silver-copper alloys, *Lupis, Metall. Trans. B* 8B (1977) 691, <https://doi.org/10.1007/BF02658644>.
- [58] W. Krause, F. Sauerwald, M. Michalke, Die Oberflächenspannung geschmolzener Metalle und Legierungen Die Oberflächenspannung von Gold, Zink, Gold-Kupfer-, Silber-Kupfer- und Eisenlegierungen, *Z. Anorg. Allg. Chem.* 181 (1929) 353, <https://doi.org/10.1002/zaac.19291810133>.
- [59] P. Lu, M. Chandross, T.J. Boyle, B.G. Clark, P.T. Vianco, Equilibrium Cu-Ag nanoalloy structure formation revealed by in situ scanning transmission electron

- microscopy heating experiments, *Apl. Mater.* 2 (2014), 022107, [https://doi.org/10.1063/1.4866052\(022107-1-022107-6\)](https://doi.org/10.1063/1.4866052(022107-1-022107-6)).
- [60] A.T. Dinsdale, SGTE data for pure elements, *Calphad* 15 (1991) 317–425, [https://doi.org/10.1016/0364-5916\(91\)90030-N](https://doi.org/10.1016/0364-5916(91)90030-N).
- [61] S. Wagner, G. Sodeck, A. Neckel, Thermodynamic excess quantities of liquid binary silver-copper by mass spectrometry, *High Temp. Sci.* 3 (1971) 481–490.